LANGMUIR

pubs.acs.org/Langmuir Article

Layer-by-Layer Assembly of Photosystem I and PEDOT:PSS Biohybrid Films for Photocurrent Generation

Kody D. Wolfe,[$] Avi Gargye,[$] Faustin Mwambutsa, Long Than, David E. Cliffel, and G. Kane Jennings*

Cite This: *Langmuir* 2021, 37, 10481−10489 Read Online

ACCESS | Metrics & More | Article Recommendations | Supporting Information

ABSTRACT: The design of electrode interfaces to achieve efficient electron transfer to biomolecules is important in many bioelectrochemical processes. Within the field of biohybrid solar energy conversion, constructing multilayered Photosystem I (PSI) protein films that maintain good electronic connection to an underlying electrode has been a major challenge. Previous shortcomings include low loadings, long deposition times, and poor connection between PSI and conducting polymers within composite films. Here, we show that PSI protein complexes can be deposited into monolayers within a 30 min timespan by leveraging the electrostatic interactions between the protein complex and the poly(3,4-ethylenedioxythiophene)-polystyrenesulfonate (PEDOT:PSS) polymer. Further, we follow a layer-by-layer (LBL) deposition procedure to produce up to 9-layer pairs of PSI and PEDOT:PSS with highly reproducible layer thicknesses as well as distinct changes in surface composition. When tested in an electrochemical cell employing ubiquinone-0 as a mediator, the photocurrent performance of the LBL films increased linearly by 83 ± 6 nA/cm^2 per PSI layer up to 6-layer pairs. The 6-layer pair samples yielded a photocurrent of 414 ± 13 nA/cm^2, after which the achieved photocurrent diminished with additional layer pairs. The turnover number (TN) of the PSI−PEDOT:PSS LBL assemblies also greatly exceeds that of drop-casted PSI multilayer films, highlighting that the rate of electron collection is improved through the systematic deposition of the protein complexes and conducting polymer. The capability to deposit high loadings of PSI between PEDOT:PSS layers, while retaining connection to the underlying electrode, shows the value in using LBL assembly to produce PSI and PEDOT:PSS bioelectrodes for photoelectrochemical energy harvesting applications.

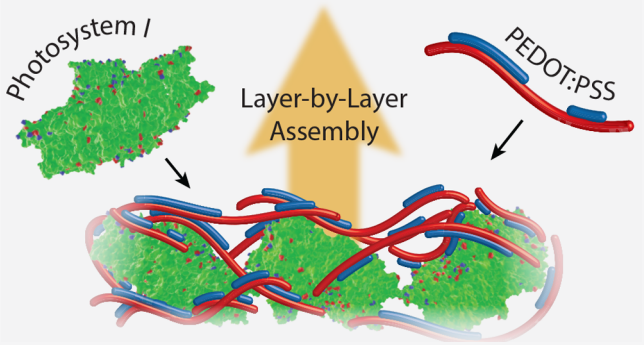

INTRODUCTION

Pressing environmental challenges are pushing researchers to develop solar energy conversion systems with lower manufacturing demands, affordable and abundant materials, and high efficiencies. One source for inspiration is photosynthesis, the natural process that plants and other organisms use to convert solar energy into usable chemical energy. In photosynthesis, electrons are shuttled along the electron transport chain by the Photosystem I (PSI) and Photosystem II (PSII) protein complexes.[1] PSI acts as a biological photodiode by collecting photons, funneling their energy to the P_{700} reaction center, and transferring excited electrons c.a. 10 nm from P_{700} to the F_B iron cluster. Due to its nanoscale size, natural abundancy, and ability to energize electrons with nearly perfect internal quantum efficiency, the PSI protein complex has been investigated with significant interest in recent developments of biohybrid photoelectrochemical cells.[2−4]

In PSI-based electrodes and devices, PSI protein complexes are deposited as a monolayer or a multilayer film onto a variety of electrode materials. Several methods to immobilize PSI have been reported, including self-assembly, vacuum-assisted drop-casting, dip-coating, Langmuir monolayer transfer, spin-coating, and copolymerization among others.[5−14] Regardless of the deposition technique, the desired characteristics of a PSI film include high connectivity between protein complexes, high loading of protein complexes, and good connection between the active layers and the electrode. Conducting polymers offer a promising route toward improving the connectivity between the electrically insulating proteins. Conducting polymers fall into two classes, intrinsic or electron conducting polymers and redox polymers, and both types have been used in conjunction with PSI. Zhao et. al and Badura et al. developed osmium-based redox hydrogels and hydrogel films for use with PSI, showing the promise of redox polymers in the field and resulting in their continued use in recent efforts.[11,12,15,16]

Received: May 25, 2021
Revised: July 14, 2021
Published: August 24, 2021

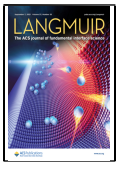

https://doi.org/10.1021/acs.langmuir.1c01385
Langmuir 2021, 37, 10481−10489

Dervishogullari et al. used a polyviologen redox polymer as an electron transport layer and Yehezkeli et al. used two redox active polymers to create layered films incorporating PSI and PSII.[17,18] Intrinsic conducting polymers have also been successfully used in thylakoid membrane-based bioelectrodes and as bulk conducting layers in PSI solid state devices.[19−21]

Recently, our group has focused on incorporating PSI within intrinsically conducting polymer matrices to fabricate PSI-based biohybrid electrodes.[13,14,17] Gizzie et al. electropolymerized aniline in the presence of PSI to entrap it, creating an active layer for a PSI-polyaniline bioelectrode, and later a solid state biophotovoltaic device.[14,22] An impressive increase in photocurrent is provided by PSI at low loadings (14.5 ± 2.7 nmol PSI/cm^3); however, obtaining higher loadings of PSI in the devices was not demonstrated due to limitations in the electropolymerization process.[3] In another project, Robinson et al. vapor deposited poly(3,4-ethylenedioxythiophene) (PEDOT) throughout a multilayer of PSI and concluded that PEDOT acted as an extension of the electrode, decreasing photocurrent attenuation for PSI farther from the electrode.[13] Unfortunately, when this grafting technique was used with densely packed PSI multilayers, only a small amount of PEDOT was able to grow near the electrode, limiting electrical connectivity. To address the issue of increasing PSI loading while retaining the beneficial properties of using intrinsically conducting polymer entrapment, we have leveraged electrostatic interactions between PSI and poly(3,4-ethylenedioxythiophene)-polystyrenesulfonate (PEDOT:PSS) to enable the preparation of layered PSI−PEDOT:PSS films. PEDOT:PSS is a polymer salt with PEDOT acting as the positively charged polycation and PSS acting as the polyanion.[23] PSI also bears a mixed charge in solution due to the varied functional groups on its surface. Figure 1 schematically depicts the surface of the PSI protein complex and illustrates the position of primary amines and carboxylic acids that contribute a majority of PSI's mixed surface charge. At pH = 7.0 the primary amines (blue) yield a local positive charge while the carboxylic acids (red) yield a local negative charge.[24]

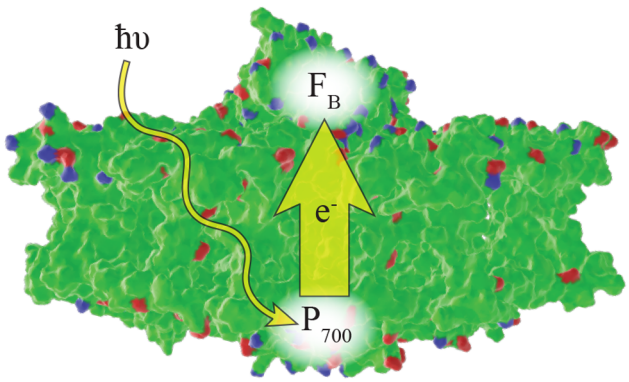

Figure 1. A schematic highlighting PSI's surface-exposed primary amines (blue) and carboxylic acids (red). At pH = 7.0, surface amines yield a local positive charge while carboxylic acids yield a negative charge. The primary amines shown are present in lysine residues while the carboxylic acids are contributed by aspartic and glutamic acid residues. The exposed functional groups on PSI were created using the PyMol molecular visualization software and structural data of Amunts et al.[24]

One method for creating composite films based on electrostatic interactions is layer-by-layer (LBL) deposition, where films are created by adsorbing nanoscale layers of material with alternating charges. LBL deposition has proven useful for a variety of applications such as membrane fabrication, electrochromism, and biomaterials.[25−29] The benefits of LBL assembly include nanoscale-control of the film thickness, ease of preparation and scalability, high degrees of reproducibility, and high achievable loadings of biomolecules.[26,30] Several researchers have used LBL deposition to couple PSI/PSII or bacterial photosynthetic reaction centers with polyelectrolytes and examined photocurrents.[28−32] Yehezkeli et al. fabricated up to 3 bilayers of poly benzyl viologen redox polymer-based LBL films with PSI.[18] The authors did not observe an increase in performance beyond 3 layers of PSI, which they attribute to electrical perturbations causing a loss of communication between the active protein and redox polymer. Stieger et al. used DNA as a polyelectrolyte to build self-assembled PSI:cytochrome c (cyt c) films.[32] The DNA polyelectrolyte was used to improve the stability of PSI and cyt c coassembled films and the results showed that the high performing electrodes were also stable for many days if stored in dry conditions.[32] This study highlights the importance of the polyelectrolyte on improving loading and stability of active components in biohybrid layered assemblies.

PEDOT:PSS has been studied as a conductive layer in PSI biohybrid films previously. Using a spin-coating technique, Barhom et al. incorporated PEDOT:PSS layers of unreported thickness as an electrode atop PSI multilayers and Kazemzadeh et al. used PEDOT:PSS as an interfacial layer between PSI and indium tin oxide (ITO) to improve the performance of solid state PSI devices.[20,21] Both of these studies capitalized on PEDOT:PSS's flexibility and electrical conductivity to improve the connection between PSI layers and electrodes. Based on the previous successes, our goal is to leverage electrostatic interactions between PSI and PEDOT:PSS to combat limitations with low PSI loadings and ill-defined electrode-conducting polymer interfaces through the fabrication and testing of PSI−PEDOT:PSS LBL films.

In this work, alternating layers of PEDOT:PSS and PSI are deposited onto aminoethanethiol (AET) monolayers on gold electrodes as shown in Figure 2. The LBL method circumvents constraints from our group's previous methods for creating PSI/conducting polymer assemblies. It ensures both high PSI loading within the film and protein/conducting polymer interactions throughout the film. During the LBL process, PEDOT:PSS first electrostatically binds to the AET monolayer, producing a thin film of PEDOT:PSS on the electrode. Next, the mixed charge functional groups on PSI's surface promote the deposition of a well-packed PSI monolayer, creating a bilayer or one layer pair. The deposition is repeated to produce many layer pairs. We then show that through mediated electron transfer (MET) via ubiquinone-0, a linear increase in photocurrent production is achieved with the addition of each layer pair up to a threshold level of 6-layer pairs and that the PSI−PEDOT:PSS LBL films greatly outperform densely packed PSI multilayer films when photocurrent is normalized to protein loading.

EXPERIMENTAL SECTION

Photosystem I Extraction. Photosystem I was extracted from spinach (*Spinacia* oleracea) following a previously described procedure.[33−35] Briefly, thylakoid membranes were isolated through mechanical maceration, filtration, and centrifugation. Thylakoid membranes were then lysed using Triton X-100 (Sigma), releasing

https://doi.org/10.1021/acs.langmuir.1c01385
Langmuir 2021, 37, 10481−10489

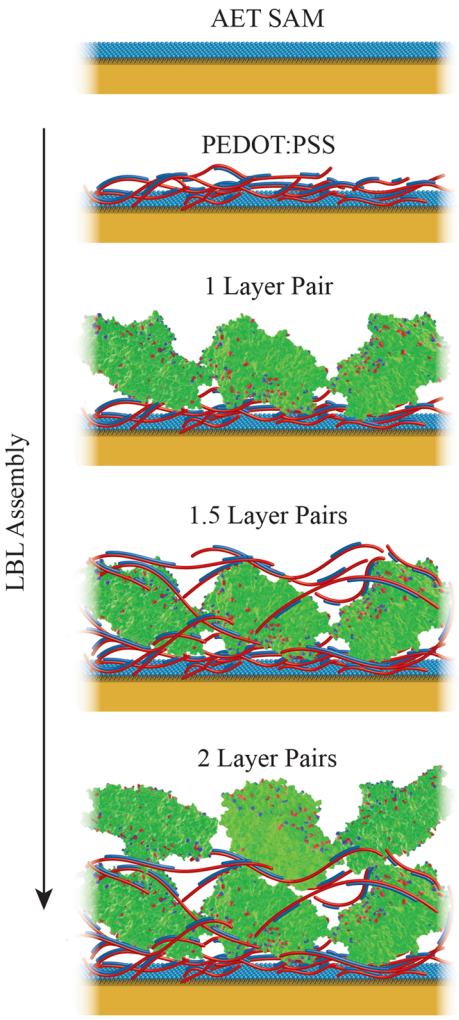

Figure 2. Schematic of LBL assembly procedure showing the depositions steps required to prepare 2-layer pairs.

PSI proteins complexes, and centrifuged once again to separate PSI within the supernatant from other miscellaneous cell material within the pellet. The surfactant also serves to solubilize the protein complex. Ion affinity chromatography was used to further purify the PSI solution. PSI is collected at an approximate concentration of 0.5 mg PSI/mL in 200 mM sodium phosphate buffer (pH = 7.0, Sigma-Aldrich) containing 1 wt % Triton X-100 (Sigma) and stored at −80 °C until use. The extraction procedure has been adapted from Shiozawa et al., who showed detailed analyses of the extraction product with similar yields reported herein.[35] Presence and activity of PSI complexes in solution were verified via UV−vis absorbance spectroscopy. The concentration of the PSI solution (0.5 mg PSI/mL) was determined using a P_{700} reaction site quantification procedure reported by Baba et al.[33]

PSI−PEDOT:PSS Layer-by-Layer Deposition. Chromium (10 nm) and gold (125 nm) were sequentially deposited onto silicon (100) wafers, via physical vapor deposition as described previously.[7] Gold-coated wafers were cut into 1.5 × 1.4 cm^2 or 2.3 × 1.4 cm^2 samples and cleaned with three alternating rinses of ethanol and deionized water. Samples were then dried under a stream of N_2 and placed into a solution of 1 mM aminoethanethiol (AET) (Thermo Scientific) in ethanol for 1 h. The result is a positively charged amine-terminated self-assembled monolayer (SAM) on the gold surface. Next, samples were again rinsed with ethanol and dried under N_2. For the LBL deposition solutions, PEDOT:PSS solution (Sigma-Aldrich, 1.1 wt %) was diluted to 0.5 mg/mL, and 0.15 M NaCl was added to the diluted PEDOT:PSS solution. Aliquots of PSI solution were used as extracted (0.5 mg PSI/mL in 200 mM sodium phosphate buffer at pH = 7.0 and containing 1 w.t.% Triton X-100). The AET SAM-modified gold substrates were first exposed to the PEDOT:PSS solution for 15 min and then to the PSI solution for 30 min. After each deposition step, the samples were excessively rinsed with deionized water and dried under N_2. The depositions of PEDOT:PSS and PSI were performed repeatedly until the desired number of bilayers was reached.

Individual Layer Thickness Measurements. Ellipsometric measurements were obtained on a JA Woollam Co. M-2000VI variable angle spectroscopic ellipsometer with WVASE32 software for modeling. Each sample was measured at two incident angles of 65° and 75° using a 632 nm HeNe laser. Film thickness was fit from these measurements by using a one-term Cauchy layer model with a refractive index of 1.45.

Water Contact Angles. Contact angles of deionized water in ambient conditions were measured on static water drops (1 μL) using a Rame-Hart goniometer. The needle remained inside the liquid drop during measurements.

Fourier Transform Infrared Spectroscopy. Phase-modulated infrared reflectance absorbance spectroscopy (PM-IRRAS) of the LBL films was conducted using a Bruker Tensor 27 Fourier transform infrared spectrometer with a liquid nitrogen-cooled, mercury−cadmium-telluride detector and an incident beam angle of 80° from the substrate surface normal.

Electrochemical Impedance Spectroscopy. Electrochemical impedance spectroscopy (EIS) was conducted on a CHI 660 potentiostat. A three-electrode cell was used with a platinum counter electrode, Ag/AgCl reference electrode (CH Instruments), and the LBL-coated gold sample as the working electrode using a custom-built sample holder. The electrochemically accessible area was constrained to an exposed area of 0.21 cm^2. All measurements were performed in an aqueous solution of 100 mM KCl (Fisher Chemical). EIS tests were performed from 10000 to 0.1 Hz at the sample's open circuit potential and a potential amplitude of 5 mV.

Photochronoamperometry. Photochronoamperometry (PCA) was performed on a CHI 660 potentiostat. The sample of interest was used as the working electrode along with a Ag/AgCl reference and a platinum mesh counter electrode. All electrolytes contained 100 mM KCl in addition to any electrochemical mediator (mentioned where applicable). Both methyl viologen (Acros-Organics) and ubiquinone-0 (2,3-dimethoxy-5-methyl-1,4-benzoquinone from Acros-Organics) were tested at a concentration of 2 mM. For all PCA data the open circuit potential of the sample was first measured in the dark, and the sample was held at the measured open-circuit potential during the photocurrent measurement. The sample was then illuminated with a 100 mW/cm^2 white light source for some time interval (typically 20 s) before the light was turned off.

Potentiometry and Photopotentiometry. Potentiometric measurements were performed similarly to the photochronoamperometry tests. A 3-electrode electrochemical cell was used with a gold or modified-gold working electrode, a Ag/AgCl reference electrode, and a platinum counter electrode. In all potentiometric tests, the cell was allowed to reach equilibrium before collecting data. The establishment of equilibrium was determined by monitoring the open circuit potential (OCP).

■ RESULTS AND DISCUSSION

During the preparation of the LBL films, advancing contact angle measurements were taken to observe the evolution of film surface composition. The exposed functional groups of PEDOT:PSS and PSI result in a change in contact angle with each layer of the deposition (Figure 3.A). The positively charged amine-terminated SAM yields a reproducible contact angle below 40° due to the strong interaction of water with the charged surface that provides a low solid−liquid interfacial free energy. The deposition of the first layer of PEDOT:PSS does not significantly change the observed contact angle. The

https://doi.org/10.1021/acs.langmuir.1c01385
Langmuir 2021, 37, 10481−10489

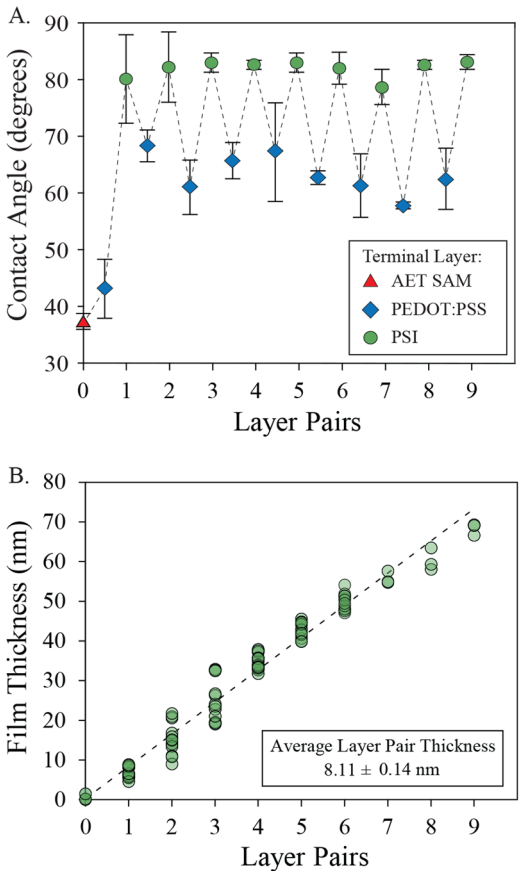

Figure 3. (A) Advancing contact angle measurements taken with deionized water after each deposition step in the LBL assembly. B.) Total film thickness for all whole layer pair samples, obtained via spectroscopic ellipsometry. Note that whole layer pair samples are terminated by PSI. Decreased opacity of the markers in panel B indicate overlapping data points.

dramatic increase in contact angle upon PSI deposition is due to the complex, amphiphilic character of PSI, which contains a hydrophobic "belt" that is typically embedded within the thylakoid membrane.[24] Contact angles for PSI monolayers have been reported as high as 90°, so the values of >80° here are consistent with a surface dominated by the protein.[36] After the PSI surface was exposed to a solution of PEDOT:PSS, the contact angle drops from ∼80° to ∼60°, indicating the presence of the more hydrophilic polymer at the surface. This contact angle trend is repetitive throughout the LBL deposition steps, signifying that the respective material is adsorbed via each deposition step and that the film maintains an adequate charge to attract the next layer.[37] This consistent deposition behavior is typical of well-behaved LBL systems. On average, PEDOT:PSS layers deposited atop PSI have a contact angle of 61° ± 9°, and PSI layers deposited atop PEDOT:PSS have an average contact angle of 82° ± 5°. Spun cast homogeneous PEDOT:PSS films have been reported to provide water contact angles of 25° because the free charges associated with the sulfonate and thiophene groups provide strong ion-dipole interactions with water.[38] In LBL films, the contact angles of water on PEDOT:PSS vary widely from 20° to 80° based on layer thickness, counterion of the salt, and composition of the other polyion.[39,40] The discrepancy shown between the first and subsequent PEDOT:PSS layers here is attributed to the different sublayers, a highly charged AET surface versus a more hydrophobic PSI layer, in which each may be partially exposed. These different sublayers would also affect the structure of the PEDOT:PSS layer. Water is known to be sensitive to surface groups located within ∼0.3−0.4 nm of the outermost surface.[41] Thus, given the average thicknesses of the polymer layers (1−2 nm, shown in Figure S.1) and the sensitivity of contact angle to the sublayer, the contact angles suggest that intermixing occurs between the polymer and protein layers. A schematic of this behavior is shown in Figure 2, in which the PEDOT:PSS polymer penetrates the PSI layers.

The film thickness was also measured between each deposition step using spectroscopic ellipsometry (Figure 3B). In classical LBL films, alternating layers of oppositely charged polyions are deposited, and the resulting layers are considered as intermingling charged domains with thicknesses on the order of 1−3 nm per layer pair.[26] The PSI and PEDOT:PSS case is much more complex due to the sheer size of the PSI protein complex and the mixed-charge nature of both PSI and PEDOT:PSS.[24] The thickness of the PEDOT:PSS and PSI composite films grows linearly by 8.11 ± 0.14 nm with each additional layer pair (Figure 3.B). Based on the reproducibility of ellipsometric thickness measurements across many samples, we believe that the films are much more uniform than their thicker drop-casted counterparts.[15] While the step height for whole layer pairs is highly reproducible, the height change of individual PEDOT:PSS or PSI layers is typically within the bounds of error of the previous layer (Figure S.1). Figure S.1 shows that, qualitatively, PEDOT:PSS layers increase the thickness much less than the PSI layers, as is expected based on their molecular sizes. The PEDOT:PSS layers increase the film thickness on the order of 1−2 nm while the PSI layers add approximately 6−7 nm. The increase in film thickness during PSI deposition is consistent with the formation of a dense PSI monolayer after only a short deposition time of 30 min.[6] For comparison, Faulkner et al. required 48 h for solution phase assembly to deposit a similar thickness of PSI.[6] We believe the faster deposition onto the PEDOT:PSS polymer is due to the favorable electrostatic interactions between the mixed charges present on PSI along with the positive charge of the PEDOT moiety and the negative PSS counteranion.

FTIR spectroscopy was used to confirm the presence of both PSI and PEDOT:PSS in the film as layers were assembled. PSI's characteristic amide I and amide II peaks appear prominently at 1664 cm^{-1} (I) and 1547 cm^{-1} (II) in both the 1- and 8-layer pair samples shown in Figure 4. The observed amide I and amide II bands align well with the PSI spectra presented by Robinson et al.,[13] indicating that PSI is present, but whether in layer 1 or all inclusive, PSI exhibits a secondary structure that is consistent with that of redox-active PSI used in multilayer and polymer composite films. The peaks observed at 1009 cm^{-1} (VII) and 1036 cm^{-1} (VI) are attributed to PSS's S-phenyl bond, and the broad peak at 1182 cm^{-1} (IV) is attributed to PSS's S=O vibration.[42−44] The peaks at 1128 and 1219 cm^{-1}(III) correspond to PEDOT's C−O−C bond.[42,44,45] These peaks, characteristic of PEDOT:PSS, are present in the 1- and 8-layer pair samples as well, indicating that PSI deposition does not remove either PEDOT or PSS during LBL deposition. The peaks corresponding to PSS and PEDOT at 1182 and 1219 cm^{-1}, respectively, grow further apart as layers of PSI and the polymer are added repetitively to the film (Figure S2 and Table S1). Specifically, the S=O peak (PSS) shifts from 1182 to 1173 cm^{-1} and the C−O−C peak

https://doi.org/10.1021/acs.langmuir.1c01385
Langmuir 2021, 37, 10481−10489

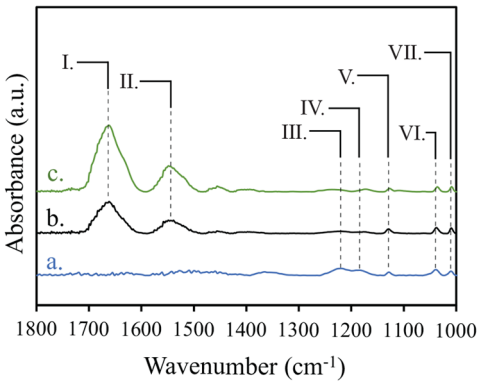

Figure 4. (a) FTIR spectra of a single layer of PEDOT:PSS atop an AET monolayer shown at 25X intensity, (b) a 1-layer pair LBL film shown at 8X intensity, and (c) an 8-layer pair LBL film shown at 1X intensity. Dashed lines and Roman numerals indicate the positions of key absorbance peaks, as described in the text.

(PEDOT) shifts from 1219 to 1232 cm^{-1} between the PEDOT:PSS film and the 8-layer pair film. These peak shifts may be an indication of attractive intermolecular interactions between the polymer and PSI. Studies have noted peak shifts during LBL deposition as a result of electrostatic or dipole−dipole interactions.[46,47] Collectively, these results show that LBL films are indeed prepared with PSI and PEDOT:PSS with all three components present and, thus, indicate attractive interactions between the protein and the charged polymer.

The photoelectrochemical activity of the LBL films was studied using photochronoamperometry (PCA). For all PCA experiments, the open circuit potential (OCP) was first measured in the dark, and the measured OCP value for each individual sample was recorded and used as the applied potential in the PCA experiment. By beginning the test at OCP, the background current is near zero, and any increase in current upon illumination is directly due to reactions within the film and, ultimately, at the electrode surface. We began by investigating various electrochemical mediator species and testing control samples consisting of a single PEDOT:PSS layer upon an AET SAM (Figures S.3 and S.4). A near zero photocurrent response was found for all control samples that did not contain PSI (Figure S.4). Concerning the electrochemical mediators, both methyl viologen and ubiquinone-0 were tested, and all mediator solutions were used at ambient conditions. For films consisting of three-layer pairs, anodic photocurrents were observed for all mediators. The ubiquinone-0 mediator produced higher photocurrents and was therefore chosen for further study of PSI activity in the LBL films. The films were tested under aerobic conditions and, therefore, the lower photocurrent produced by methyl

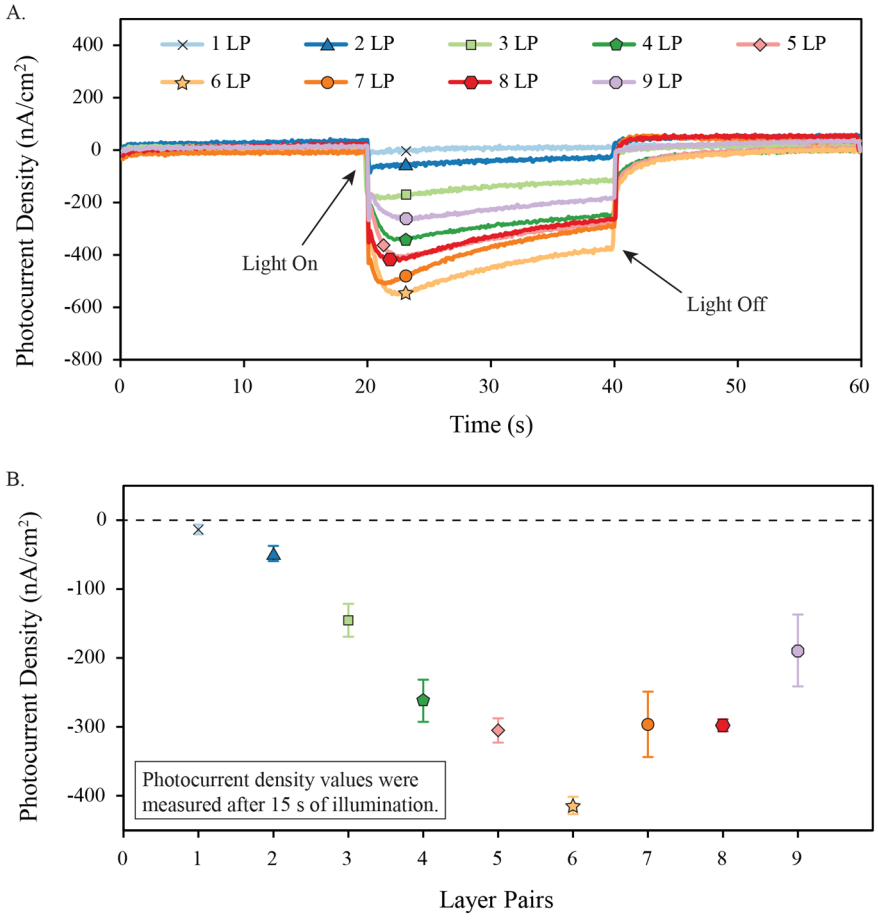

Figure 5. Photochronoamperometry (PCA) data for 1- through 9-layer pair samples of PSI and PEDOT:PSS LBL assemblies. (A) Representative PCA curves for each layer pair where the samples were illuminated from 20 to 40 s by a 100 mW/cm^2 white light source. (B) Average photocurrent response after 15 s of illumination (at t = 35 s in panel A). Each data point represents 3 independently prepared samples (n = 3). All PCA data were obtained at open circuit potential (measured in the dark) and in the presence of 2 mM ubiquinone-0 and 100 mM KCl.

https://doi.org/10.1021/acs.langmuir.1c01385
Langmuir 2021, 37, 10481−10489

viologen may be due to competing methyl viologen oxidation by dissolved oxygen species.[48] The behavior of ubiquinone-0 as an electrochemical mediator for PSI was studied and the results are summarized in the following paragraphs and shown in Supporting Information Figures S.5-S.8. Ubiquinone-0 has been used as a mediator in PSI bioelectrodes and was shown to mitigate damage by reactive oxygen species during photocurrent production by Zhao et al.[49] Additionally, Friebe et al. have studied direct reductions of ubiquinone-0 by reaction centers of photosynthetic protein complexes.[50]

In the LBL films, ubiquinone-0 facilitates anodic photocurrent generation by shuttling electrons from PSI to the PEDOT:PSS or the underlying electrode. We determined that the PEDOT:PSS interlayers act as a conductive framework, aiding in electron transfer to the underlying electrode and improving the photocurrent production of the LBL films. PEDOT:PSS acting as a conductive framework is supported by electrochemical impedance spectroscopy (EIS), which showed no observable increase in impedance with the addition of layer pairs (Figure S.9). Cyclic voltammetry of the tested mediators (Figure S.5) shows that, in comparison to methyl viologen, ubiquinone-0 has a greater overpotential vs the F_B^- reaction site and partakes in a two-electron transfer that is pH independent.[51] We believe the greater overpotential and the additional transferred electron result in greater photocurrent with ubiquinone-0 in comparison to methyl viologen.

The driving force behind the ubiquinone-0 mediated photocurrent is the production of excess reduced species by PSI in the presence of dissolved oxygen. Previous studies by our group have shown that PSI can exhibit imbalanced reaction kinetics with electrochemical mediators, which result in anodic photocurrent generation when an excess of reduced mediator is produced near the electrode.[52] The OCP of the LBL films (Figure S.6) is first set by the production of some reduced species by PSI in the dark. To illustrate this finding, we show that immediately upon introduction of PSI to a ubiquinone-0 solution, the OCP shifts negatively due to the production of reduced ubiquinone-0 in the presence of dissolved oxygen (Figure S.7). Next, upon illumination, a further increase in the concentration of reduced species is observed (Figure S.8). These results agree with recent reports on the importance of dissolved oxygen in PSI bioelectrodes and the use of ubiquinone-0 as an electron acceptor from PSI.[3,49,50,53] In summary, PSI creates an excess of reduced ubiquinone-0 upon illumination and an anodic current is realized when the excess reduced ubiquinone-0 is oxidized at either the PEDOT:PSS interlayers or the electrode surface.

The LBL films were tested for photocurrent performance as soon as possible after the terminal PSI layer was deposited. Figure 5 shows the PCA testing of samples with up to 9-layer pairs. Figure 5A shows a representative PCA curve for each sample type, and Figure 5B gives a summary of the PCA results where n = 3 independently prepared samples for each number of layer pairs. The photocurrent of the LBL films increased in a linear manner up to 6-layer pairs, where a maximum value of 414 ± 13 nA/cm^2 was achieved, and then decreased with additional layers.

The shape of the photocurrent curves indicates that two electron transfer processes are occurring. A photocurrent spike and diffusional loss is observed, but the spike is hidden by a gradual increase in photocurrent. The spike behavior is typical of mediated electron transfer (MET) in a PSI film as reported by Robinson et al.[52] However, the diffusional loss or "diffusional tail" does not follow the typical shape for MET. Instead, an increase in current is observed in the first 2 s of illumination, followed by a gradual decrease after 2 s. We attribute this unique shape to a "sawtooth" photocurrent limitation which has been observed in solid-state PSI devices.[14] In a sawtooth response, the photocurrent increases gradually up to a maximum value and does not show signs of diffusional losses. An overlay of a "sawtoothed" photocurrent response and a typical MET response (a spike followed by a diffusional loss) yields the photocurrent shape observed in the LBL assemblies. We believe the combination of the photocurrent response shapes is due to the two modes of electron transfer. The first is MET from PSI to the PEDOT:PSS or underlying electrode (diffusional response) and the second is electron transfer through the PEDOT:PSS conductive framework (sawtooth).

We attribute the photocurrent maximum achieved at 6-layer pairs to charge carrier trapping within the outermost PEDOT:PSS domains of the film.[26,54−56] Charge carrier trapping has been observed in model LBL systems such as polybithiophene and polyviologen films.[56] As the number of layer pairs increases in the PSI−PEDOT:PSS films, electrons that have been excited by PSI may no longer have an energetically favorable path to the electrode due to film imperfections, inhomogeneity, and the resistance associated with the PSI interlayers. Instead of contributing to the observed photocurrent, these electrons will be trapped throughout the PEDOT:PSS framework where they impact the polymer's redox state and may lower conductivity. Based upon the trend in Figure 5.B, we believe the charging effect must increase as the distance from the electrode to the outermost layer increases and that charging within one layer can alter electron transfer from nearby layers. EIS data for 6- through 9-layer pairs (Figure S.9) shows that no barrier effect to ion transfer is introduced with the additional layers, suggesting that the charging effect occurs only during photocurrent production. The inability to collect these electrons and an overall decrease in film conductivity results in a trade-off in performance at higher numbers of layer pairs, yielding a maximum photocurrent density between 5 and 7-layer pairs.

Through a least-squares linear regression we determined that each additional layer pair (between 1- and 6-layer pairs) yields an increase of 83 ± 6 nA/cm^2 of anodic photocurrent. In comparison to previously reported PSI monolayers, which yielded approximately 90 nA/cm^2 when densely packed in a single monolayer on gold, the LBL system achieves a similar performance with each layer pair until saturation is reached at 6-layer pairs.[6] To our knowledge, this is the highest number of distinct PSI layers deposited in a layered film. Yehezkeli et al. reported a maximum in performance after just 3 layers of PSI deposition.[18] The ability to systematically build individual layers of PSI and conducting polymer is encouraging for the development of improved connectivity and higher loadings of PSI in films for both liquid electrochemical cells and solid-state PSI devices. To ensure the observed photocurrent response can be directly attributed to the incorporation of PSI, an additional control test was conducted by layering PSI that had been deactivated by ultraviolet light along with PEDOT:PSS to produce a 3-layer pair deactivated PSI control. Figure S.10 shows absorbance spectra of extracted PSI and PSI which was exposed to UV light for 2 and 4 h, thereby losing its ability to specifically absorb red and blue light. Figure S.11 shows the

https://doi.org/10.1021/acs.langmuir.1c01385
Langmuir 2021, 37, 10481−10489

near zero photocurrent obtained from the 3-layer pair deactivated PSI sample in comparison to a representative 3-layer pair PSI sample.

The PSI LBL films exhibit a large photocurrent response for such a thin PSI film (~50 nm thickness at 6-layer pairs). To better understand how individual PSI complexes are performing in the LBL films, we analyzed the performance on a per PSI basis by calculating the turnover number (TN). The TN is calculated using eq 1 below and describes the photocurrent normalized to the quantity of PSI in the film

$$TN\left(\frac{mol_{e^-}}{s*mol_{PSI}}\right) = \frac{i_{PCA}\left(\frac{A}{cm^2}\right)}{C_{PSI}\left(\frac{mol_{PSI}}{cm^2}\right)*F\left(\frac{C}{mol_{e^-}}\right)} \quad (1)$$

Shown in Figure 6, the TN was calculated from PCA data and is plotted for each number of layer pairs. When compared in terms of TN, a similar performance is achieved between 4- and 6-layer pairs. Thus, the negative impacts of loss of charge trapping result in similar TNs for 4-, 5-, and 6-layer pairs before the TN decreases above 6-layer pairs. These results show that a trade-off in performance is being made gradually, beginning at approximately 4-layer pairs. We also performed studies of densely packed, drop-casted PSI multilayer films atop a PEDOT:PSS film in the presence of 2 mM ubiquinone-0. Shown in red in Figure 6, multilayer films of PSI achieve a TN of 0.03 ± 0.01 $mol_{e^-}/(s\ mol_{PSI})$, an order of magnitude lower than the PSI–PEDOT:PSS LBL films which achieve 0.34 ± 0.03 $mol_{e^-}/(s\ mol_{PSI})$ for 4- to 6-layer pairs. Therefore, the LBL films not only increase the achievable loading of PSI but also enable more current to be produced by each PSI complex in the film when compared to a less organized PSI multilayer.

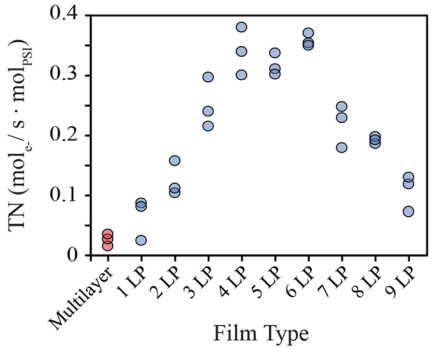

Figure 6. Turnover numbers for devices based on photocurrent performance and quantity of PSI in the film. For multilayer films, the quantity of PSI was determined based on the concentration and volume of PSI solution deposited and for LBL films the amount of PSI was determined based on the number of densely packed monolayers present.

Limitations of the current system include low light absorbance by such thin films and the MET by ubiquinone-0, both of which limit the amount of photocurrent. Circumventing the latter will require further study on the use of mixed mediators for enhanced electron and hole extraction from PSI. Nonetheless, the LBL films show linear increases in mediated photocurrent generation by ubiquinone-0 for each layer pair added up to 6-layer pairs, and the achieved TN is also an order of magnitude greater than that of a densely packed PSI multilayer. These results along with the highly reproducible nature of the LBL assemblies show great promise for producing very thin and high performing PSI and PEDOT:PSS bioelectrodes.

CONCLUSIONS

The rapid deposition of alternating layers of PSI and PEDOT:PSS via LBL deposition was leveraged to produce layered assemblies up to 9-layer pairs thick. The ability to deposit these PSI–PEDOT:PSS LBL films is due to the favorable electrostatic interactions between the mixed charge surfaces of the PSI protein complex (Figure 1) and the PEDOT:PSS polymer. The LBL assemblies yielded alternating changes in contact angle throughout the deposition process along with a highly reproducible layer pair thickness of 8.11 ± 0.14 nm. An increase in photocurrent density of 83 ± 6 nA/cm^2 was observed with each additional layer pair from 1- to 6-layer pairs. The linear enhancement of the achieved photocurrent peaked at 6-layer pairs, producing 414 ± 13 nA/cm^2, and then decreased with additional layer pairs. We attribute the decrease in performance to charge carrier trapping within the outermost PEDOT:PSS layers due to an increase in resistance to electron transfer across or through the proteinaceous interlayers. The LBL films greatly outperform densely packed PSI multilayer films in terms of the turnover number (TN), proving that LBL assembly of PSI with an intrinsically conducting polymer provides benefits beyond increasing areal loading of the protein complex. Our results highlight the LBL process as an efficient and controllable means of depositing PSI films and shows promise for the tailoring of the PSI and PEDOT:PSS LBL system to produce a variety of biohybrid photovoltaic device architectures in the future.

ASSOCIATED CONTENT

Supporting Information

The Supporting Information is available free of charge at https://pubs.acs.org/doi/10.1021/acs.langmuir.1c01385.

Partial layer pair thicknesses, IR peak shifts and assignments, photochronoamperometry controls and mediator tests, electrochemical impedance spectra of 6–9 layer pair films, and controls with deactivated Photosystem I (PDF)

AUTHOR INFORMATION

Corresponding Author

G. Kane Jennings – *Department of Chemical and Biomolecular Engineering, Vanderbilt University, Tennessee 37235-1604, United States;* orcid.org/0000-0002-3531-7388; Email: kane.g.jennings@vanderbilt.edu

Authors

Kody D. Wolfe – *Interdisciplinary Materials Science & Engineering Program, Vanderbilt University, Tennessee 37235-0106, United States;* orcid.org/0000-0002-6452-0107

Avi Gargye – *Department of Chemical and Biomolecular Engineering, Vanderbilt University, Tennessee 37235-1604, United States*

Faustin Mwambutsa – *Department of Chemical and Biomolecular Engineering, Vanderbilt University, Tennessee 37235-1604, United States*

Long Than − *Department of Chemical and Biomolecular Engineering, Vanderbilt University, Tennessee 37235-1604, United States*

David E. Cliffel − *Department of Chemistry, Vanderbilt University Nashville, Tennessee 37235-1822, United States;* orcid.org/0000-0001-8756-106X

Complete contact information is available at: https://pubs.acs.org/10.1021/acs.langmuir.1c01385

Author Contributions

[$]The manuscript was written through contributions of all authors. All authors have given approval to the final version of the manuscript. These authors contributed equally.

Funding

The work presented herein was funded by United States Department of Agriculture grant number 2019−67021−29857.

Notes

The authors declare no competing financial interest.

■ ACKNOWLEDGMENTS

The authors would like to thank the United States Department of Agriculture (2019-67021-29857) and the Vanderbilt Undergraduate Summer Research Program (for A.G.) for funding this work, as well as the Vanderbilt Institute for Nanoscale Science & Engineering (VINSE) for the use of analytical instrumentation. The authors thank Prof. Paul Laibinis for insightful discussion.

■ ABBREVIATIONS

PSI, Photosystem I; PEDOT:PSS, poly(3,4-ethylenedioxythiophene)-polystyrenesulfonate; LBL, layer-by-layer; PSII, Photosystem II; PEDOT, poly(3,4-ethylenedioxythiophene); ITO, indium tin oxide; AET, aminoethanethiol; MET, mediated electron transfer; SAM, self-assembled monolayer; PM-IRRAS, phase-modulated infrared reflectance absorbance spectroscopy; EIS, electrochemical impedance spectroscopy; PCA, photochronoamperometry; OCP, open-circuit potential; TN, turnover number

■ REFERENCES

(1) Nelson, N.; Junge, W. Structure and Energy Transfer in Photosystems of Oxygenic Photosynthesis. *Annu. Rev. Biochem.* **2015**, *84*, 659−683.

(2) Nguyen, K.; Bruce, B. D. Growing green electricity: Progress and strategies for use of Photosystem I for sustainable photovoltaic energy conversion. *Biochim. Biophys. Acta, Bioenerg.* **2014**, *1837*, 1553−1566.

(3) Wolfe, K. D.; Dervishogullari, D.; Passantino, J. M.; Stachurski, C. D.; Jennings, G. K.; Cliffel, D. E. Improving the stability of photosystem I−based bioelectrodes for solar energy conversion. *Curr. Opin. Electrochem.* **2020**, *19*, 27−34.

(4) Friebe, V. M.; Frese, R. N. Photosynthetic reaction center-based biophotovoltaics. *Curr. Opin. Electrochem.* **2017**, *5*, 126−134.

(5) Ciesielski, P. N.; Faulkner, C. J.; Irwin, M. T.; Gregory, J. M.; Tolk, N. H.; Cliffel, D. E.; Jennings, G. K. Enhanced Photocurrent Production by Photosystem I Multilayer Assemblies. *Adv. Funct. Mater.* **2010**, *20*, 4048−4054.

(6) Faulkner, C. J.; Lees, S.; Ciesielski, P. N.; Cliffel, D. E.; Jennings, G. K. Rapid Assembly of Photosystem I Monolayers on Gold Electrodes. *Langmuir* **2008**, *24*, 8409−8412.

(7) Kincaid, H. A.; Niedringhaus, T.; Ciobanu, M.; Cliffel, D. E.; Jennings, G. K. Entrapment of Photosystem I within Self-Assembled Films. *Langmuir* **2006**, *22* (19), 8114−8120.

(8) Manocchi, A. K.; Baker, D. R.; Pendley, S. S.; Nguyen, K.; Hurley, M. M.; Bruce, B. D.; Sumner, J. J.; Lundgren, C. A. Photocurrent Generation from Surface Assembled Photosystem I on Alkanethiol Modified Electrodes. *Langmuir* **2013**, *29*, 2412−2419.

(9) Mukherjee, D.; May, M.; Vaughn, M.; Bruce, B. D.; Khomami, B. Controlling the Morphology of Photosystem I Assembly on Thiol-Activated Au Substrates. *Langmuir* **2010**, *26* (20), 16048−16054.

(10) Yan, X.; Faulkner, C. J.; Jennings, G. K.; Cliffel, D. E. Photosystem I in Langmuir−Blodgett and Langmuir−Schaefer Monolayers. *Langmuir* **2012**, *28* (42), 15080−15086.

(11) Wang, P.; Frank, A.; Zhao, F.; Szczesny, J.; Junqueira, J. R. C.; Zacarias, S.; Ruff, A.; Nowaczyk, M. M.; Pereira, I. A. C.; Rögner, M.; Conzuelo, F.; Schuhmann, W. Closing the Gap for Electronic Short-Circuiting: Photosystem I Mixed Monolayers Enable Improved Anisotropic Electron Flow in Biophotovoltaic Devices. *Angew. Chem., Int. Ed.* **2021**, *60* (4), 2000−2006.

(12) Zhao, F.; Wang, P.; Ruff, A.; Hartmann, V.; Zacarias, S.; Pereira, I. A. C.; Nowaczyk, M. M.; Rögner, M.; Conzuelo, F.; Schuhmann, W. A photosystem I monolayer with anisotropic electron flow enables Z-scheme like photosynthetic water splitting. *Energy Environ. Sci.* **2019**, *12* (10), 3133−3143.

(13) Robinson, M. T.; Simons, C. E.; Cliffel, D. E.; Jennings, G. K. Photocatalytic photosystem I/PEDOT composite films prepared by vapor-phase polymerization. *Nanoscale* **2017**, *9*, 6158−6166.

(14) Gizzie, E. A.; Scott Niezgoda, J.; Robinson, M. T.; Harris, A. G.; Jennings, G. K.; Rosenthal, S. J.; Cliffel, D. E. Photosystem I-polyaniline/TiO2solid-state solar cells: Simple devices for biohybrid solar energy conversion. *Energy Environ. Sci.* **2015**, *8*, 3572−3576.

(15) Zhao, F.; Sliozberg, K.; Rögner, M.; Plumeré, N.; Schuhmann, W. The Role of Hydrophobicity of Os-Complex-Modified Polymers for Photosystem 1 Based Photocathodes. *J. Electrochem. Soc.* **2014**, *161*, 3035−3041.

(16) Badura, A.; Guschin, D.; Kothe, T.; Kopczak, M. J.; Schuhmann, W.; Rögner, M. Photocurrent generation by photosystem 1 integrated in crosslinked redox hydrogels. *Energy Environ. Sci.* **2011**, *4*, 2435−2440.

(17) Dervishogullari, D.; Gizzie, E. A.; Jennings, G. K.; Cliffel, D. E. Polyviologen as Electron Transport Material in Photosystem I-Based Biophotovoltaic Cells. *Langmuir* **2018**, *34* (51), 15658−15664.

(18) Yehezkeli, O.; Tel-Vered, R.; Michaeli, D.; Nechushtai, R.; Willner, I. Photosystem I (PSI)/Photosystem II (PSII)-Based Photo-Bioelectrochemical Cells Revealing Directional Generation of Photocurrents. *Small* **2013**, *9* (17), 2970−2978.

(19) Efrati, A.; Lu, C.-H.; Michaeli, D.; Nechushtai, R.; Alsaoub, S.; Schuhmann, W.; Willner, I. Assembly of photo-bioelectrochemical cells using photosystem I-functionalized electrodes. *Nat. Energy* **2016**, *1* (2), 15021.

(20) Kazemzadeh, S.; Riazi, G.; Ajeian, R. Novel Approach of Biophotovoltaic Solid State Solar Cells Based on a Multilayer of PS1 Complexes as an Active Layer. *ACS Sustainable Chem. Eng.* **2017**, *5*, 9836−9840.

(21) Barhom, H.; Carmeli, C.; Carmeli, I. Fabrication of Electronic Junctions between Oriented Multilayers of Photosystem I and the Electrodes of Optoelectronic Solid-State Devices. *J. Phys. Chem. B* **2021**, *125* (3), 722−728.

(22) Gizzie, E. A.; LeBlanc, G.; Jennings, G. K.; Cliffel, D. E. Electrochemical Preparation of Photosystem I−Polyaniline Composite Films for Biohybrid Solar Energy Conversion. *ACS Appl. Mater. Interfaces* **2015**, *7* (18), 9328−9335.

(23) Leaf, M. A.; Muthukumar, M. Electrostatic Effect on the Solution Structure and Dynamics of PEDOT:PSS. *Macromolecules* **2016**, *49* (11), 4286−4294.

(24) Amunts, A.; Toporik, H.; Borovikova, A.; Nelson, N. Structure determination and improved model of plant photosystem I. *J. Biol. Chem.* **2010**, *285*, 3478−3486.

(25) Crespilho, F.; Zucolotto, V.; Oliveira, O. Electrochemistry of Layer-by-Layer Films: a review. *Int. J. Electrochem. Sci.* **2006**, *1*, 194−214.

(26) DeLongchamp, D. M.; Kastantin, M.; Hammond, P. T. High-Contrast Electrochromism from Layer-By-Layer Polymer Films. *Chem. Mater.* **2003**, *15* (8), 1575−1586.

(27) Lvov, Y. M.; Lu, Z.; Schenkman, J. B.; Zu, X.; Rusling, J. F. Direct Electrochemistry of Myoglobin and Cytochrome P450cam in Alternate Layer-by-Layer Films with DNA and Other Polyions. *J. Am. Chem. Soc.* **1998**, *120* (17), 4073−4080.
(28) Ventrella, A.; Catucci, L.; Placido, T.; Longobardi, F.; Agostiano, A. Photosystem II based multilayers obtained by electrostatic layer-by-layer assembly on quartz substrates. *J. Bioenerg. Biomembr.* **2014**, *46* (3), 221−228.
(29) Zhao, J.; Liu, B.; Zou, Y.; Xu, C.; Kong, J. Photoelectric conversion of photosynthetic reaction center in multilayered films fabricated by layer-by-layer assembly. *Electrochim. Acta* **2002**, *47* (12), 2013−2017.
(30) Cao, Y.; Chen, D.; Wu, X.; Kong, J.; Zou, Y.; Xu, C. Probing Electron Transfer of the Redox Species in Wild-Type RC Protein and its Pigment-Replaced Mutants Re-Constituted in Self-Assembly Monolayers. *Anal. Lett.* **2001**, *34* (5), 713−725.
(31) Kong, J.; Sun, W.; Wu, X.; Deng, J.; Lu, Z.; Lvov, Y.; Desamero, R. Z. B.; Frank, H. A.; Rusling, J. F. Fast reversible electron transfer for photosynthetic reaction center from wild type Rhodobacter sphaeroides re-constituted in polycation sandwiched monolayer film. *Bioelectrochem. Bioenerg.* **1999**, *48* (1), 101−107.
(32) Stieger, K. R.; Ciornii, D.; Kölsch, A.; Hejazi, M.; Lokstein, H.; Feifel, S. C.; Zouni, A.; Lisdat, F. Engineering of supramolecular photoactive protein architectures: the defined co-assembly of photosystem I and cytochrome c using a nanoscaled DNA-matrix. *Nanoscale* **2016**, *8*, 10695−10705.
(33) Baba, K.; Itoh, S.; Hastings, G.; Hoshina, S. Photoinhibition of Photosystem I electron transfer activity in isolated Photosystem I preparations with different chlorophyll contents. *Photosynth. Res.* **1996**, *47*, 121−130.
(34) Wolfe, K. D.; Dervishogullari, D.; Stachurski, C. D.; Passantino, J. M.; Kane Jennings, G.; Cliffel, D. E. Photosystem I Multilayers within Porous Indium Tin Oxide Cathodes Enhance Mediated Electron Transfer. *ChemElectroChem* **2020**, *7* (3), 596−603.
(35) Shiozawa, J. A.; Alberte, R. S.; Thornber, J. P. The P700-chlorophyll a-protein: Isolation and some characteristics of the complex in higher plants. *Arch. Biochem. Biophys.* **1974**, *165* (1), 388−397.
(36) Ciesielski, P. N.; Scott, A. M.; Faulkner, C. J.; Berron, B. J.; Cliffel, D. E.; Jennings, G. K. Functionalized Nanoporous Gold Leaf Electrode Films for the Immobilization of Photosystem I. *ACS Nano* **2008**, *2*, 2465−2472.
(37) Decher, G.; Eckle, M.; Schmitt, J.; Struth, B. Layer-by-layer assembled multicomposite films. *Curr. Opin. Colloid Interface Sci.* **1998**, *3* (1), 32−39.
(38) Duc, C.; Malliaras, G. G.; Senez, V.; Vlandas, A. Long-term ageing of PEDOT:PSS: wettability Study. *Synth. Met.* **2018**, *238*, 14−21.
(39) Tang, Z.; Donohoe, S. T.; Robinson, J. M.; Chiarelli, P. A.; Wang, H.-L. Film formation, surface character, and relative density for electrochromic PEI/(PSS:PEDOT) multilayered thin films. *Polymer* **2005**, *46* (21), 9043−9052.
(40) Jurin, F. E.; Buron, C. C.; Martin, N.; Monney, S.; Filiâtre, C. Electrical conductivity enhancement and wettability modification of (PDDA/PEDOT:PSS)n multilayer film. *Thin Solid Films* **2018**, *664*, 33−40.
(41) Laibinis, P. E.; Bain, C. D.; Nuzzo, R. G.; Whitesides, G. M. Structure and Wetting Properties of ω-Alkoxy-n-alkanethiolate Monolayers on Gold and Silver. *J. Phys. Chem.* **1995**, *99* (19), 7663−7676.
(42) Seekaew, Y.; Lokavee, S.; Phokharatkul, D.; Wisitsoraat, A.; Kerdcharoen, T.; Wongchoosuk, C. Low-cost and flexible printed graphene−PEDOT:PSS gas sensor for ammonia detection. *Org. Electron.* **2014**, *15* (11), 2971−2981.
(43) Yoo, D.; Kim, J.; Kim, J. H. Direct synthesis of highly conductive poly(3,4-ethylenedioxythiophene):poly(4-styrenesulfonate) (PEDOT:PSS)/graphene composites and their applications in energy harvesting systems. *Nano Res.* **2014**, *7* (5), 717−730.
(44) Friedel, B.; Keivanidis, P. E.; Brenner, T. J. K.; Abrusci, A.; McNeill, C. R.; Friend, R. H.; Greenham, N. C. Effects of Layer Thickness and Annealing of PEDOT:PSS Layers in Organic Photodetectors. *Macromolecules* **2009**, *42* (17), 6741−6747.
(45) Bahry, T.; Cui, Z.; Deniset-Besseau, A.; Gervais, M.; Sollogoub, C.; Bui, T.-T.; Remita, S. An alternative radiolytic route for synthesizing conducting polymers in an organic solvent. *New J. Chem.* **2018**, *42* (11), 8704−8716.
(46) de Barros, A.; Ferreira, M.; Constantino, C. J. L.; Ferreira, M. Nanocomposites based on LbL films of polyaniline and sodium montmorillonite clay. *Synth. Met.* **2014**, *197*, 119−125.
(47) de Barros, A.; Constantino, C. J. L.; da Cruz, N. C.; Bortoleto, J. R. R.; Ferreira, M. High performance of electrochemical sensors based on LbL films of gold nanoparticles, polyaniline and sodium montmorillonite clay mineral for simultaneous detection of metal ions. *Electrochim. Acta* **2017**, *235*, 700−708.
(48) Zhao, F.; Hardt, S.; Hartmann, V.; Zhang, H.; Nowaczyk, M. M.; Rögner, M.; Plumeré, N.; Schuhmann, W.; Conzuelo, F. Light-induced formation of partially reduced oxygen species limits the lifetime of photosystem 1-based biocathodes. *Nat. Commun.* **2018**, *9*, 1973.
(49) Zhao, F.; Ruff, A.; Rögner, M.; Schuhmann, W.; Conzuelo, F. Extended Operational Lifetime of a Photosystem-Based Bioelectrode. *J. Am. Chem. Soc.* **2019**, *141*, 5102−5106.
(50) Friebe, V. M.; Swainsbury, D. J. K.; Fyfe, P. K.; van der Heijden, W.; Jones, M. R.; Frese, R. N. On the mechanism of ubiquinone mediated photocurrent generation by a reaction center based photocathode. *Biochim. Biophys. Acta, Bioenerg.* **2016**, *1857*, 1925−1934.
(51) Gulaboski, R.; Markovski, V.; Jihe, Z. Redox chemistry of coenzyme Q - a short overview of the voltammetric features. *J. Solid State Electrochem.* **2016**, *20* (12), 3229−3238.
(52) Robinson, M. T.; Cliffel, D. E.; Jennings, G. K. An Electrochemical Reaction-Diffusion Model of the Photocatalytic Effect of Photosystem I Multilayer Films. *J. Phys. Chem. B* **2018**, *122* (1), 117−125.
(53) Morlock, S.; Subramanian, S. K.; Zouni, A.; Lisdat, F. Scalable Three-Dimensional Photobioelectrodes Made of Reduced Graphene Oxide Combined with Photosystem I. *ACS Appl. Mater. Interfaces* **2021**, *13* (9), 11237−11246.
(54) Abruna, H. D.; Denisevich, P.; Umana, M.; Meyer, T. J.; Murray, R. W. Rectifying interfaces using two-layer films of electrochemically polymerized vinylpyridine and vinylbipyridine complexes of ruthenium and iron on electrodes. *J. Am. Chem. Soc.* **1981**, *103* (1), 1−5.
(55) Ruths, J.; Essler, F.; Decher, G.; Riegler, H. Polyelectrolytes I: Polyanion/Polycation Multilayers at the Air/Monolayer/Water Interface as Elements for Quantitative Polymer Adsorption Studies and Preparation of Hetero-superlattices on Solid Surfaces. *Langmuir* **2000**, *16* (23), 8871−8878.
(56) Hillman, A. R.; Mallen, E. F. Electroactive bilayers employing conducting polymers. Part 2. Speciation by in situ spectroscopy. *J. Chem. Soc., Faraday Trans.* **1991**, *87* (14), 2209−2217.

https://doi.org/10.1021/acs.langmuir.1c01385
Langmuir 2021, 37, 10481−10489